Contrib Mineral Petrol (2005) 149: 576–590
DOI 10.1007/s00410-005-0665-8

ORIGINAL PAPER

I. Tonguç Uysal · Arthur J. Mory · Suzanne D. Golding
Robert Bolhar · Kenneth D. Collerson

Clay mineralogical, geochemical and isotopic tracing of the evolution of the Woodleigh impact structure, Southern Carnarvon Basin, Western Australia

Received: 27 October 2003 / Accepted: 18 March 2005

Abstract Chaotically structured diamictite from the inner ring syncline surrounding the central uplift of the Woodleigh impact structure contains shocked metamorphic and impact melt-rock fragments, largely derived from Ordovician and Devonian target sandstones. Coarse illite fractions (<2 μm) from the sandstones containing no K-feldspar yield K–Ar ages of around 400 Ma, whereas the K–Ar ages of authigenic clays of >0.2 μm fractions from the diamictite without smectite and K-feldspar cluster around 360 Ma, consistent with Rb–Sr data. Crystallisation of newly formed illite in the impact melt rock clasts and recrystallisation of earlier formed illite in the sandstone clasts preserved in the diamictite, are attributed to impact-induced hydrothermal processes in the Late Devonian. The illitic clays from the diamictite and from the sandstones have very similar trace element compositions, with significantly enriched incompatible lithophile elements, which increase in concentrations correlatively with those of the compatible ferromagnesian elements. The unusual trace element associations in the clays may be due to the involvement of hot gravity-driven basinal fluids that interacted with rocks of the Precambrian craton to the east of the study area, or with such material transported and reworked in the studied sedimentary succession.

Introduction

The interpretation of impact-related geological phenomena using mineralogic, geochemical and isotopic studies is far from straightforward. Rocks affected by an impact largely preserve their pre-impact geochemical and isotopic composition because differently shocked and unshocked mineralogical phases may be found juxtaposed at a sub-millimetric scale (e.g., Deutsch and Schärer 1994). Therefore, isotopic analyses of whole-rocks or clastic components may be insufficient to derive satisfactory explanations of impact related events. Alternatively, clays are excellent paleotemperature and paleohydrologic indicators, and their isotopic and geochemical signatures can provide information about specific physico-chemical conditions during low-temperature geological events (Clauer and Chaudhuri 1995; Uysal et al. 2001a, 2003). Clay mineral authigenesis has been well documented in impact-induced or post-impact alteration processes (e.g., Allen et al. 1982; Kirsimäe et al. 2002; Dypvik et al. 2003), and can provide a powerful tool to trace the post-impact evolution of impact structures. When reconstructing thermal and fluid flow history related to impact events, it is essential to distinguish precisely impact-related local processes from regional geological events. Therefore, it is important to take into account the regional thermal and fluid flow history of the sedimentary basin to evaluate the data unambiguously—aspects that are addressed in the present study on the Woodleigh impact structure. The aim is to constrain the evolution of the Southern Carnarvon Basin in relation to the Woodleigh impact event, with particular emphasis on the physico-chemical conditions during post-impact alteration processes. Constraints are derived from

Communicated by J. Hoefs

I. Tonguç Uysal (✉) · S. D. Golding
Earth Sciences, University of Queensland,
Brisbane, 4072, QLD, Australia
E-mail: t.uysal@earth.uq.edu.au
Tel.: +6-17-33652130
Fax: +6-17-33651277

A. J. Mory
Geological Survey of Western Australia,
100 Plain St., East Perth, WA,
6004, Australia

R. Bolhar · K. D. Collerson
Advanced Centre for Queensland
University Research Excellence (ACQUIRE),
University of Queensland, Brisbane, 4072, QLD, Australia

mineralogic, isotopic and trace element analyses of clay minerals from clastic sedimentary rocks of the Southern Carnarvon basin both within and away from the Woodleigh impact structure.

Geological background and sampling

The Gascoyne Platform in the Southern Carnarvon basin, Western Australia, contains up to 5,000 m of Ordovician–Lower Devonian strata covered by a thin Cretaceous–Cainozoic succession. The Woodleigh impact structure, lying largely within the Gascoyne Platform (Fig. 1), has been recognised from a multi-ring Bouguer gravity anomaly and shows well-preserved shock metamorphic features (Mory et al. 2000; Iasky et al. 2001; Reimold et al. 2003). The structure consists of deformed, domed Devonian to Ordovician sedimentary strata, and has an uplifted granitoid basement below a Cretaceous section at its centre in borehole Woodleigh-1 (Fig. 2). Woodleigh-2A located 15 km to the west penetrated a Cretaceous section similar to that in Woodleigh-1, but overlying the lacustrine Lower Jurassic Woodleigh Formation (223–521.3 m), unnamed diamictite (521.3–587.2 m), unnamed breccia (587.2–600.85 m), and Silurian platform carbonate rocks (Coburn Formation, Dirk Hartog Group, 600.85–618.3 m), in which the well was terminated (Mory et al. 2001; Fig. 2). The unnamed breccia consists mainly of dolomite clasts apparently derived from the underlying Silurian formation. The diamictite (referred to as a paraconglomerate by Mory et al. 2001) consists mainly of large fragments of deformed and shocked components of Ordovician–Devonian sandstones and devitrified glassy materials (see below). A large number of the samples are from the diamictite because it contains altered impact rock fragments that can provide valuable information on impact-induced hydrothermal processes. Since the majority of the diamictite components appear to be derived from impact-affected sandstones, core samples from Ordovician and Devonian sandstones were also analysed from Yaringa-1 and Yaringa East-1 drill cores of within the Woodleigh structure (Figs. 1, 2) as well as their equivalents outside the Woodleigh structure in Coburn-1 (to the south), Dirk Hartog-17B (to the west) and Wandagee-1 (to the north; Fig. 1). Comparison of the results obtained from the diamictite and the sandstones is crucial to assess if any mineralogical and geochemical changes are related either to the Woodleigh impact, or to the regional evolution of the basin.

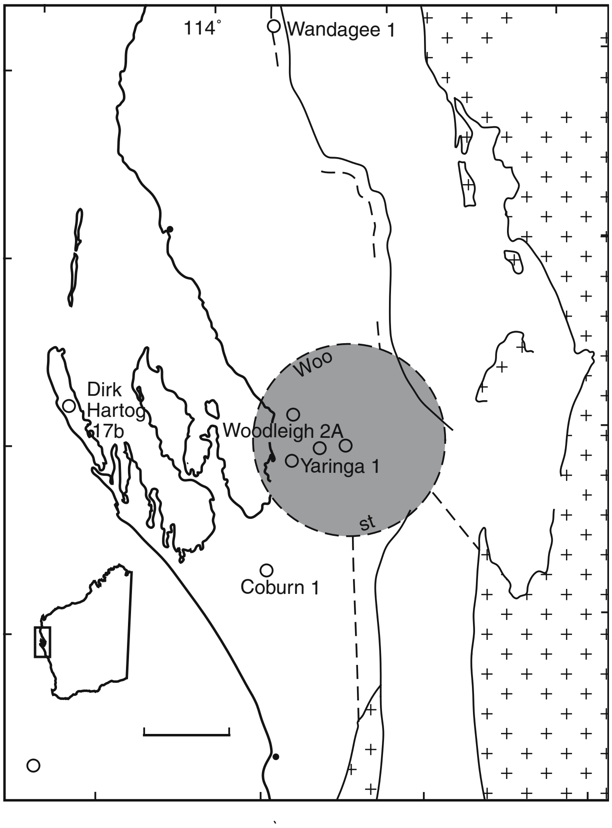

Fig. 1 Location map of the study area and the analysed samples

Analytical methods

Mineralogic studies were performed using X-ray diffraction (XRD), and optical and scanning electron microscopy (SEM). The XRD analyses were carried out on a X-ray diffractometer equipped with parallel beam geometry and CuKα radiation, operated at 40 kV and 40 mA at a scanning rate of 1°2θ/min. SEM analyses were carried out with a scanning electron microscope equipped with EDAX Si (Li) energy dispersive spectrometer (EDS). XRD and SEM analyses were performed in the Centre for Microscopy and Microanalyses at the University of Queensland.

The samples were prepared for separation of the clay fraction by gently crushing the rocks to sand size, followed by disaggregation in distilled water using an ultrasonic bath. Different clay size fractions were obtained by centrifugation, and the decanted suspensions were placed on a glass slide. Following XRD analysis of air-dried samples, the oriented clay-aggregate mounts were placed in an ethylene–glycol atmosphere at 30–40°C overnight prior to additional XRD analyses. The illite crystallinity (IC) or Kübler index is defined as the width of the first order illite basal reflection (10 Å peak) at half height and expressed in $\Delta 2\theta$ values (Frey 1987).

The Ar isotopic composition was determined by isotope dilution using ^{38}Ar as a tracer. Ages were calculated after correcting for machine mass discrimination and system blanks using the decay constants of Steiger and Jäger (1977). The K_2O content of the samples was determined using an inductively coupled plasma optical emission spectrometer with an accuracy better than 1%. Errors include all uncertainties in the measurement of the isotope ratios and K contents and are quoted in the

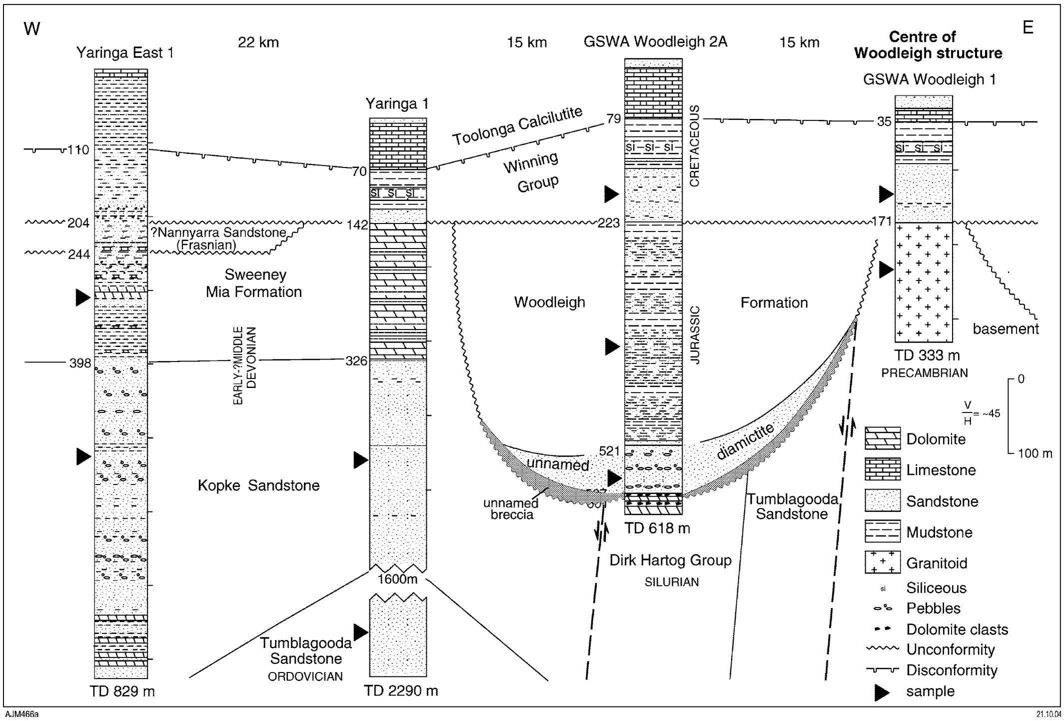

Fig. 2 Stratigraphic correlation of the boreholes sampled in the Woodleigh impact structure. *Arrows* show the sampled formations

text as ±2σ. Ar isotopic results were controlled by analysing the international GLO-glauconite standard, with an average of $11.14 \pm 0.15 \times 10^{-10}$ mole/g (2σ, $n = 6$) standard (cf. 11.09×10^{-10} mole/g, Odin et al. 1982) of radiogenic ^{40}Ar. K–Ar analyses were carried out in the laboratory of Earth Sciences of UQ.

For the Rb–Sr dating, illite clay separates were leached for 15 min at room temperature in 1 *N* distilled HCl. Samples were spiked with ^{85}Rb–^{84}Sr and dissolved in a mixture of distilled HF and HNO_3. The Sr-enriched fraction was separated using cation exchange resin. Sr isotopic ratios were measured on a thermal ionisation mass spectrometer. Sr was loaded in 1 *N* HNO_3 on a Ta single filament. Sr isotopic ratios were corrected for mass discrimination using ^{86}Sr/^{88}Sr = 0.1194. Long-term (6 years) reproducibility of the NBS SRM 987 ($n = 442$) is 0.710249 ± 28 and the Pacific Ocean limestone standard EN-1 ($n = 561$) is 0.709176 ± 32 (2σ). During the course of this study, the value obtained for the ^{87}Sr/^{86}Sr ratio of standard NBS 987 was 0.710242 ± 12 (2σ, $n = 6$). Rb–Sr analyses were performed in the ACQUIRE laboratory.

For trace element analysis, rock standards and clay fractions were dissolved in teflon beakers on a hot plate and whole-rocks in high pressure bombs in an oven. Analyses were performed on an ICP-MS in the ACQUIRE laboratory. Instrument operating conditions follow Eggins et al. (1997). Duplicate hot plate digestions of W-2 (Table 5) were used for external calibration and the ACQUIRE long term average for AGV-1 (representing 32 analyses of 11 digestions over 8 years) is also shown in Table 5.

Results

Petrography

Petrographic analyses of the diamictite indicate that it is sourced largely from siliciclastic rocks. The largest proportion of the diamictite (~80 vol%) is probably derived from the Ordovician Tumblagooda Sandstone, which is the thickest pre-impact sedimentary formation, and possibly also from Devonian Kopke Sandstone. In addition, the Dirk Hartog Group and possibly the Sweeney Mia Formation may have provided some siliciclastic and carbonate components. The proportion of shocked Precambrian granitoid in the diamictite is considerably less than the proportion of the siliciclastic and carbonate components (< 10 vol%).

The diamictite displays an unsorted and chaotic mix of angular to rounded clasts dispersed in a silty-sand to argillaceous matrix (Fig. 3a). Mineral clasts and matrix consist predominantly of quartz and less K-feldspar. Minor mica and carbonate grains are present. Quartz grains typically show shock metamorphic effects, especially enhanced fracturing and fragmentation or brecciation, and planar deformation features (Uysal et al. 2001b, 2002, and Fig. 3b). Diaplectic quartz glass is also present in some samples. Some rock fragments with an aphanitic texture in a micro- to cryptocrystalline matrix resemble devitrified volcanic glass and enclose Ti–Fe oxides (Fig. 3c). SEM-EDS spectra indicate that K–Al and Mg–Fe silicates are major components of the groundmass. The SEM images combined with XRD patterns reveal that these very fine-grained crystallized minerals are mainly illite, but also include chlorite,

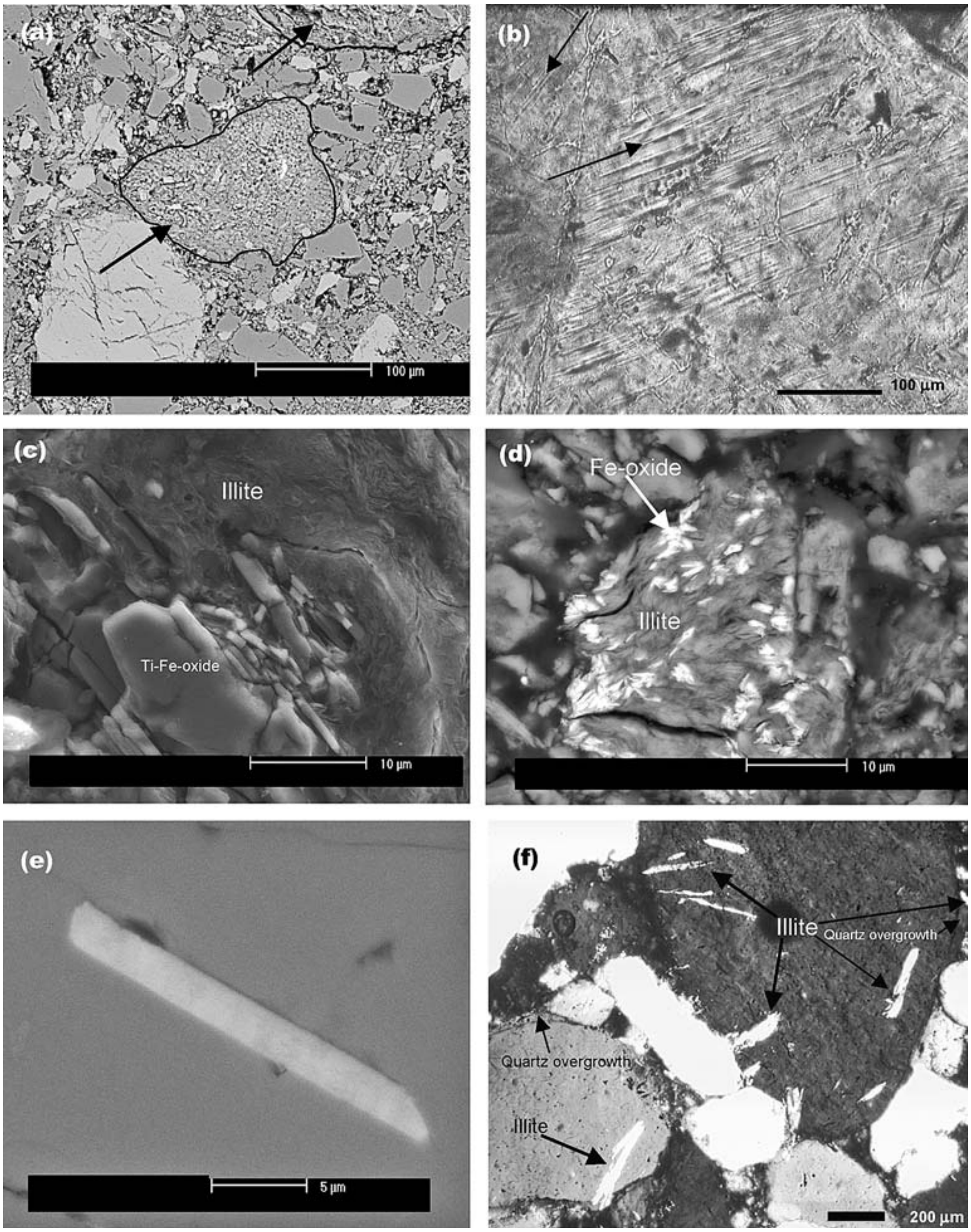

Fig. 3 SEM and thin section photomicrographs illustrating the main components of the diamictite from borehole Woodleigh-2A. **a** BSE image of sample at 585.15 m. Note the impact melt breccia at the centre and in the upper part of the image (*arrows*), surrounded by angular quartz clasts and a silty–sandy and argillaceous matrix. **b** Two sets of PDFs (*arrows*) in a quartz grain from the sample at 534.85 m. **c** SEI image of tabular crystals of a Ti-oxide mineral embedded in a groundmass consisting of platy illite formed by alteration of impact melt glass in the sample at 551.85 m. **d** BSE image of a devitrified glass component that shows hematite plates (*white*) set in an illite matrix and surrounded by angular quartz clasts in sample at 551.85 m. **e** Euhedral illite crystal precipitated within a quartz grain in the sandstone sample at 397.65 m from borehole Yaringa East-1. **f** Lath-shaped illite crystals (*arrows*) replacing quartz grains and quartz-overgrowths (*right in the upper part*) in the sandstone at 397.65 m in borehole Yaringa East-1

carbonate and quartz (Fig. 3c). Illite occurs as oriented microlites or randomly dispersed patches in thin section, and platy crystals in SEM (Fig. 3c).

The detrital components of the sandstones are dominated by quartz (~70 vol%) with minor K-feldspar (~5–20 vol%). The remainder of the sandstones consists of cements including quartz, carbonates, K-feldspar, anhydrite, halite, sylvite and Fe-oxides. Illite is present in most of the samples, usually as euhedral lath-shaped crystals precipitated within quartz grains and cement (Fig. 3d–e). Feldspars are mostly fresh and show no evidence of alteration to illite. The presence of euhedral illite crystals indicates that the illitization is due to precipitation from the circulating fluids rather than the replacement of pre-existing minerals. Previous studies have shown that illite with perfect euhedral crystals develop by neoformation from fluids at relatively high water/rock ratios (e.g., sandstones), whereas illite from rocks having low porosity and permeability (e.g., shales) forms commonly by replacement of a smectite-type precursor (Yau et al. 1988). The latter is characteristic for the solid-state transformation mechanism (Inoue et al. 1990).

Clay mineralogy

Clay mineralogy data based on XRD analysis and SEM observation indicate that illite is the main clay mineral in the diamictite and sandstone samples. Intensity ratio

(IR) values (Srodon and Eberl 1984) of illite from the diamictite are greater than one (Table 1), indicating the presence of some expandable components in these clays. However, the 001 peak position of the illite XRD patterns does not change after ethylene glycol treatment suggesting a smectite content of < 5%. Smectite is present as discrete phase in the clay fractions only in the upper part of the diamictite. Its abundance decreases with depth; it is absent below 585.15 m in Woodleigh-2A. Chlorite is present only in traces in the upper part of the section. Corrensite and chlorite-rich mixed-layered chlorite–smectite are present in the basal 2 m of the diamictite (Table 1). Many < 2 μm fractions contain non-clay minerals including quartz and K-feldspar. K-feldspar is present in most of the > 1 μm size fractions from the upper part of the diamictite and in all > 0.5 μm size fractions from the lower part of the diamictite.

There is an obvious difference in IC for the diamictite illite above and below 585.15 m in Woodleigh-2A (Table 1). The samples above yield generally uniform IC

Table 1 Clay mineralogy data

Sample depth (m)	Grain size (μm)	Smectite	Illite	Chlorite	C–S	IC (Δ2θ°)	IR
Woodleigh-2A (diamictite)							
521.65	< 2	XXX	XXX	X	–	0.55	2.71
521.65	2–1	XXX	XXX	X	–	0.52	
521.65	1–0.5	XXX	XXX	X	–	0.46	
521.65	0.5–0.2	XXX	XX	–	–	0.61	
534.85	< 2	XXX	XXX	X	–	0.51	1.87
534.85	2–1	XXX	XXX	–	–	0.57	
534.85	1–0.5	XXX	XXX	X	–	0.50	
534.85	0.5–0.2	XXX	XXX	X	–	0.60	
551.80	< 2	XX	XXX	X	–	0.56	1.57
551.80	2–1	–	XXX	–	–	0.43	
551.80	1–0.5	X	XXX	X	–	0.46	
551.80	0.5–0.2	XX	XXX	X	–	0.60	
551.90	2–0.3[a]	–	XXX	–	–	0.53	
551.90	< 0.2[a]	XX	XXX	X	–	0.84	
568.55	< 2	X	XXX	X	–	0.56	1.24
568.55	2–1	–	XXX	X	–	0.44	
568.55	1–0.5	X	XXX	X	–	0.48	
568.55	0.5–0.2	XX	XXX	X	–	0.66	
585.15	< 2	X	XXX	XX	–	0.52	1.15
585.15	2–1	–	XXX	X	–	0.44	
585.15	1–0.5	–	XXX	X	–	0.50	
585.15	0.5–0.2	X	XXX	X	–	0.59	
585.20	< 0.3[a]	–	XXX	X	XX	0.80	
586.40	< 2	–	XXX	XX	XX	0.75	2.83
586.40	2–1	–	XXX	X	XX	0.76	
586.40	1–0.5	–	XXX	X	XX	0.81	
586.40	0.5–0.2	–	XXX	XX	XX	0.81	
586.90	< 0.3[a]	–	XXX	XX	XX	0.88	
587.00	< 0.2[a]	–	XXX	X	X	0.94	
587.20	< 2	–	XXX	X	XX	0.77	1.65
587.20	2–1	–	XXX	XX	X	0.60	
587.20	1–0.5	–	XXX	X	XX	0.69	
587.20	0.5–0.2	–	XXX	XX	XX	0.82	
Yaringa-1 (sandstone)							
355-K	< 2	–	XXX	–	–	0.93	
740-K	< 2	XXX	XXX	X	–	0.75	
2,280-T	< 2	–	XXX	–	–	0.83	
Yaringa East-1 (sandstone)							
270.3-S	< 2	–	XXX	XX	–	1.1	
273.6-S	< 2	–	XXX	XX	–	1.1	
273.60	< 0.2	–	XXX	–	–	1.25	
397.65-K	< 2	–	XXX	X	–	1.45	
Coburn-1 (sandstone)							
401.8-K	< 2	–	–	XXX	–		
1,032.8-T	< 2	–	XXX	X	–	0.81	
Dirk Hartog-17B							
1,487–1,492-T	< 2	–	XXX	XX	–	0.73	
Wandagee-1							
875–876	< 2	–	XXX	–	–	0.78	
1,010.70	< 2	–	XXX	–	–	0.69	

K Kopke Sandstone, *T* Tumblagooda Sandstone, *S* Sweeney Mia Formation, *XXX* major, *XX* minor, *X* trace, – absent, *C–S* chlorite–smectite, *IC* illite crystallinity, *IR* intensity ratio (Srodon and Eberl 1984)

[a] Data from Uysal et al. (2001a, b)

values of around 0.55° 2θ whereas samples below have somewhat higher IC values of around 0.75° 2θ. The IC values for the sandstone illite, which is located further away from the central part of the Woodleigh structure (Fig. 1), are even up to 1.45° 2θ (Table 1).

K–Ar data

K–Ar ages of 17 illitic clay mineral fractions of different sizes (>2, <2, 1–0.5, 0.5–0.2, and <0.2 μm) from the diamictite and sandstones are presented in Table 2. The K–Ar dates of illite fractions from the sandstones are older compared to those from the diamictite (except two non-authigenic separates; see below). Ages from <2 μm fractions and one 1–0.5 μm fraction of the Tumblagooda Sandstone and Sweeney Mia Formation in Yaringa-1 and Yaringa East-1 fall between 398 ± 10 Ma and 416 ± 11 Ma. Two <2 μm samples from the Lower Devonian Kopke Sandstone yield K–Ar ages of 458 ± 13 Ma and 451 ± 17 Ma, respectively, which is older than the stratigraphic age of the Kopke Sandstone. According to XRD and thin section observations, the Kopke Sandstone contains a high proportion of detrital K-feldspar that probably explains the older K–Ar dates. Three <0.2 μm fractions of sandstone samples yield younger K–Ar dates ranging from 325 ± 13 Ma to 275 ± 10 Ma (Table 2).

Most illite fractions from the diamictite are mineralogically impure containing either smectite or K-feldspar that significantly affect the K–Ar ages. The only samples free from smectite and K-feldspar are the 2–1 μm fraction at 551.80 m and the <0.5 μm fractions of the lower part (below 585.15 m) of the diamictite. The 2–1 μm fraction at 551.80 m and the 0.5–0.2 μm fraction at 586.40 m give very similar dates of 365 ± 9 Ma and 367 ± 9 Ma, respectively. The 0.5–0.2 μm size fraction at 587.20 m yields a similar age of 358 ± 9 Ma. These K–Ar values are consistent with the ages of similar clays fractions (free from K-feldspar and smectite) from the diamictite that were reported previously (Uysal et al. 2001b). In the previous study, some younger K–Ar dates were reported for the <0.3 μm size fractions from the lower part of the diamictite, ranging from 352 ± 9 Ma to 320 ± 13 Ma (Uysal et al. 2001b) (Table 2). Similarly younger dates were obtained in the present study for the coarser clay fractions that contain smectite: the 1–0.5 μm and 0.5–0.2 μm fractions of sample at 551.80 m, and the 1–0.5 μm fraction of sample at 585.15 m contain high amounts of smectite (Table 1) and give K–Ar dates ranging from 347 ± 9 Ma to 331 ± 9 Ma (Table 2).

Coarse-grained fractions containing K-feldspar provide significantly different K–Ar data. One whole-rock diamictite sample (551.80 m) in which most of the clay fraction (<2 μm) had been removed by ultrasonic treatment, and the 1–0.5 μm fraction of the diamictite from 586.40 m yield virtually identical dates of 400 ± 12 Ma and 401 ± 10 Ma, respectively. This older value indicates that a K–Ar isotopic homogenisation of the coarser-grained K-bearing detrital phases was not completed during the younger thermal event. The age of ∼400 Ma is identical to the ages of illites from the Tumblagooda Sandstone and Sweeney Mia Formation (Table 2). This suggests that the coarser-grained detrital components of the diamictite could have derived from the sandstones, thereby confirming petrographic observations and trace element results.

Table 2 K–Ar data

Sample depth (m)	Grain size (μm)	K_2O (%)	$^{40}Ar_{rad}$ (%)	$^{40}Ar_{rad}$ (10^{-10} mole/g)	Age ± 2σ (Ma)
Woodleigh-2A (diamictite)					
551.80	Whole-rock[a]	0.65	81.00	4.2	400 ± 12
551.80	2–1	4.92	97.58	28.7	365 ± 9
551.80	1–0.5	5.56	93.46	30.1	342 ± 9
551.80	0.5–0.2	5.72	92.64	29.9	331 ± 9
585.15	1–0.5	5.57	92.19	30.6	347 ± 9
586.40	1–0.5	5.19	90.20	33.6	401 ± 10
586.40	0.5–0.2	5.03	88.69	29.5	367 ± 9
587.20	0.5–0.2	5.6	90.21	32	358 ± 9
Yaringa-1 (sandstone)					
355-K	< 2	6.89	84.20	51.8	458 ± 13
2280-T	< 2	8.41	87.10	54	398 ± 10
Yaringa East-1 (sandstone)					
270.3-S	< 2	6.09	79.90	39.5	402 ± 12
273.6-S	< 2	7.01	85.60	47.3	416 ± 11
273.6-S	1–0.5	6.56	84.10	43.3	408 ± 11
273.6-S	< 0.2	6.13	74.60	27.8	291 ± 10
397.65-K	< 2	7.07	68.30	52.2	451 ± 17
397.65-K	< 0.2	8.15	70.10	34.9	275 ± 10
Dirk Hartog-17B					
1487–1492-T	< 0.2	8.51	65.60	43.7	325 ± 13

K Kopke Sandstone, *T* Tumblagooda Sandstone, *S* Sweeney Mia Formation

[a] Clay content has been minimised by ultrasonic treatement

In summary, coarse illite fractions (< 2 µm) from the sandstones containing no K-feldspar yield consistent K–Ar dates around 400 Ma, and the K–Ar values of coarser authigenic clay fractions (> 0.2 µm) from the diamictite without smectite and K-feldspar cluster around 360 Ma. Finer illite fractions (< 0.2 µm) from the sandstones and the clay fractions containing smectite from the diamictite give lower K–Ar dates ranging from 347 ± 9 Ma to 275 ± 9 Ma.

There is a systematic relationship between the K–Ar dates and IC values of the illites from the sandstones and the diamictite (Fig. 4). The coarser-grained illites from the sandstones yielding higher K–Ar dates around 400 Ma (except two contaminated samples from the Kopke Sandstone) are characterised by high IC values (Fig. 4). The coarser-grained illites from the diamictite showing better crystallinity (low IC values) have younger K–Ar dates (between 367 Ma and 330 Ma). By contrast, the K–Ar dates and crystallinity values of the finest-grained (< 0.3 µm) illite from the diamictite and sandstones show an inverse relationship (Fig. 4).

Rb–Sr data

The Rb–Sr data for two untreated illite fractions (9U and 10U) with close K–Ar ages (Table 2) and 8 leachates of different illite fractions from the diamictite (Table 3) show a reasonably linear relationship with a slope corresponding to an apparent age of 362 ± 12 Ma (2σ) (Fig. 5). The Rb–Sr systematics of the illites reflects an overall coherence, which is consistent with the K–Ar data. For example, plotting only the leachate and the untreated fraction of sample 10 gives an age of 355 ± 4 Ma, which is very close to the K–Ar (358 ± 9 Ma) age of this sample. This conformity suggests that the leachate and the untreated fractions were homogeneous with respect to their Sr when illite formed at 350–360 Ma.

The initial $^{87}Sr/^{86}Sr$ value of 0.71139 ± 30 in Fig. 5 is above the seawater value (Faure 1986), which may indicate the effect of recrystallisation of detrital clay material. The recrystallisation of the detrital clays is responsible for release of some radiogenic ^{87}Sr trapped in the detrital material that may have mixed with Sr sourced from the carbonates in the diamictite inducing the high of initial $^{87}Sr/^{86}Sr$ ratio.

Table 3 Rb–Sr data for samples from the diamictite (borehole Woodleigh-2A)

Sample	Depth (m)	Grain size (µm)	Rb (ppm)	Sr (ppm)	$^{87}Rb/^{86}Sr$	$^{87}Sr/^{86}Sr \pm 2\sigma$
1L	521.65	0.5–0.2	79.7	2771	0.08	0.71182 ± 2
2L	534.85	1–0.5	109	1165	0.27	0.71248 ± 2
4L	551.80	1–0.5	81.8	1556	0.15	0.71242 ± 2
5L	551.80	0.5–0.2	41.9	1290	0.09	0.71190 ± 2
6L	551.80	0.5–0.2	56.2	1892	0.09	0.71185 ± 3
7L	551.80	1–0.5	190	3276	0.17	0.71251 ± 2
8L	585.15	0.5–0.2	73.7	1842	0.12	0.71183 ± 2
9U	586.40	0.5–0.2	169	133	3.70	0.73111 ± 1
10L	587.20	0.5–0.2	56.2	962	0.17	0.71209 ± 2
10U	587.20	0.5–0.2	176	123	4.13	0.73208 ± 1

L leachate, *U* untreated

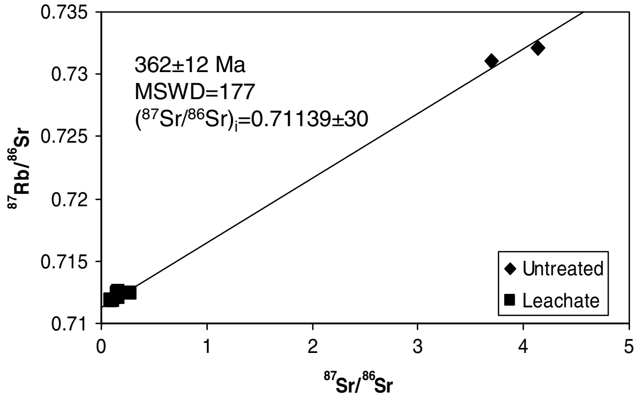

Fig. 5 Rb–Sr diagram of leachates and untreated clay fractions from the diamictite

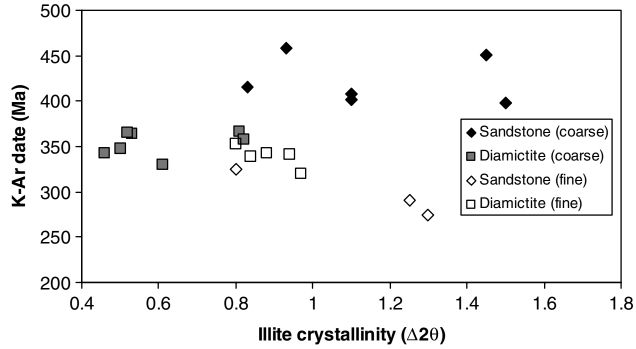

Fig. 4 Relationship between K–Ar dates and illite crystallinity for authigenic illitic clays from the diamictite and the sandstones. K–Ar data are from this study (Tables 1, 2) and Uysal et al. (2001a, b)

Major elements

Table 4 shows the major element compositions of the clay fractions (illite is the dominant or only clay mineral phase) from the diamictite (one sample) and the sandstones. Semi-quantitative element composition of one illite crystal from sample YE1-3 (Fig. 3d), based on SEM-EDS analysis, is also presented in Table 4. The illite data show considerable variation in terms of octahedral (Fe and Mg) elemental content, whereas the interlayer composition (K, Ca and Na) appears to be extremely homogeneous, with K being almost the only element filling the interlayer spaces. The latter relates to the formation (precipitation) of well-crystallised illite at a temperature above diagenesis conditions. Na is absent or present only in trace amounts, whereas, Ca shows slightly higher concentrations in some samples (Table 2).

Table 4 Major element data

Sample	Depth (m)	Grain size (μm)	Al_2O_3	CaO	Fe_2O_3	K_2O	MgO	MnO	Na_2O	P_2O_5	SiO_2	TiO_2
Woodleigh-2A (diamictite)												
W2A	551.90	< 0.2	21.03	0.60	4.80	5.83	4.53	0.01	0.68	1.19	49.49	0.10
Yaringa-1 (sandstone)												
Y1-1	355-K	< 2	19.25	< d.l.	13.85	6.89	3.45	0.03	< d.l.	0.16	47.53	0.87
Y1-3	2280-T	< 2	24.77	0.10	2.37	8.41	2.58	0.01	< d.l.	0.20	54.20	0.15
Yaringa East-1 (sandstone)												
YE1-1	270.3-S	< 2	20.55	0.07	9.70	6.09	4.96	0.03	0.04	0.04	50.63	0.76
YE1-2	273.6-S	< 2	20.37	< d.l.	5.96	7.01	4.98	0.03	0.05	0.02	52.42	0.74
YE1-2	273.6-S	1–0.5	21.31	0.07	5.78	6.56	5.57	0.03	0.05	0.02	52.85	0.86
YE1-2	273.6-S	< 0.2	20.86	0.87	4.69	6.13	6.43	0.02	0.06	0.08	55.12	0.24
YE1-3	397.65-K	< 2	19.56	< d.l.	12.05	7.07	3.28	0.02	< d.l.	0.41	49.07	1.99
YE1-3	397.65-K	< 0.2	20.57	1.01	5.43	8.15	4.22	0.01	0.09	1.04	53.31	0.25
YE1-3[a]	397.65-K		14	–	18	6	5	–	–	–	56	1
Dirk Hartog-17B												
DH	1487–1492-T	1–0.2	14.76	0.12	38.11	5.61	1.83	0.02	0.05	0.20	33.51	0.71
DH	1487–1492-T	< 0.2	23.51	1.31	5.56	8.51	3.33	0.01	0.67	0.03	50.00	0.07
Wandagee-1												
WAN9	1010.70	< 0.2	27.13	2.31	5.38	9.32	2.71	0.01	0.03	0.00	52.93	0.09
Illites of different origins (1)		< 2	24–35.6	< 0.02–0.35	0.96–7.20	7.95–9.12	0.30–2.75	–	< 0.15–0.53	–	45.7–53.6	0.20–0.69

K Kopke Sandstone, *T* Tumblagooda Sandstone, *S* Sweeney Mia Formation, *d.l.* detection limit
(1) Srodon and Eberl (1984)
[a] Semi-quantitative SEM–EDS analysis.

The most striking feature of the major-elemental illite composition is the relatively high Fe and Mg contents compared to values reported in the literature (Fig. 6). The illite from this study represents a transition from the usual composition to that of celadonite, a Fe–Mg–K-rich mica (Wise and Eugster 1964).

Trace elements

Trace element data of different clay-size fractions and some whole-rock samples from the diamictite and sandstones are given in Table 5. Trace element concentrations of the acid-leached residues and the untreated illites from the diamictite are similar, with only Th and rare earth elements (REE) being slightly enriched in the untreated clay fractions (Table 5), which might be caused by the removal leachable phases. Mean trace element concentrations of the untreated illites from the diamictite and the sandstones normalised to post-Archean average shale (PAAS, Taylor and McLennan 1985) are shown in Fig. 7. For comparison, the concentrations for one basement granitoid whole-rock sample from Woodleigh-1 in the impact centre are also presented in Fig. 7. The trace elemental compositions of the illitic clays from the diamictite and the sandstones are fairly similar, whereas the composition of the basement granitoid is distinctively different (Fig. 7).

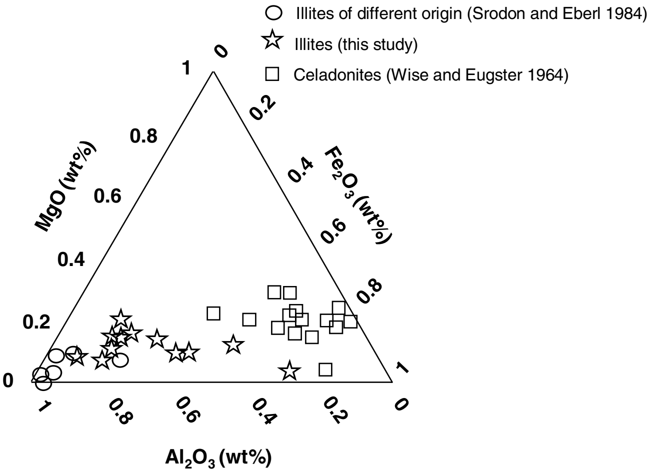

Fig. 6 Al_2O_3–MgO–Fe_2O_3 diagram for illitic clays from the diamictite and sandstones

Trace element ratios

Average trace element ratios for whole-rock samples, illite separates of the diamictite and sandstones and one basement granitoid whole-rock sample are presented in Table 6. Such element ratios are used commonly to characterise the source compositions of clastic sedimentary rocks (e.g., Taylor and McLennan 1985; Condie and Wronkiewicz 1990). Elemental ratios for the PAAS, North American shale composite (NASC), upper continental crust (UCC), Phanerozoic greywackes, illites from Paris Basin, and high-K granites from Western Australia are also presented in Table 6 for comparison. These ratios show significant differences in comparison to those of the diamictite and sandstones and the corresponding clay separates. Also the element ratios of the basement granitoid sample from the impact centre are significantly different from those of the illitic clays and their host rocks.

Table 5 Trace element data (ppm)

Sample	Depth (m)	Grain size (μm)	Li	Be	Sc	Ti	V	Cr	Co	Ni	Cu	Zn	Ga	Rb	Sr	Y	Zr	Nb	Sn	Cs	Ba	La
W-2	Standard		9.16	0.62	36.1	6355	262	92.8	44.5	70.0	103	77.0	17.4	19.8	195	20.1	87.9	7.28	1.95	0.89	170	10.5
AGV-1	Standard		10.5	2.09	12.2	6299	118	8.94	15.3	15.2	60.3	85.5	20.3	67.0	658	18.1	229	14.3	5.31	1.26	1214	38.4
RSD (%)			1.0	2.1	1.9	1.5	1.8	16.9	1.8	4.4	8.0	3.4	1.4	1.1	0.6	1.0	1.2	1.1	17.1	2.3	1.4	1.3
Woodleigh-2A (diamictite)																						
1U	521.65	0.5–0.2	38.9	5.58	12.2	1562	83.9	82.7	5.08	15.8	6.86	43.3	28.4	129	308	23.9	161	8.64	5.70	3.16	89.2	67.4
1R	521.65	0.5–0.2	40.0	6.01	12.9	1692	91.0	87.9	6.29	17.1	7.80	43.8	29.5	132	313	24.9	162	8.95	4.65	3.30	92.5	69.2
3U	551.80	2–1	26.7	2.73	6.41	1878	40.7	39.6	3.12	7.26	2.53	17.1	15.8	125	354	28.4	91.5	10.5	3.20	2.29	223	106
3R	551.80	2–1	27.9	2.79	6.31	2026	42.0	40.8	2.13	6.92	1.60	16.6	16.6	129	344	26.3	98.3	11.3	3.12	2.33	226	94.0
4R	551.80	1–0.5	34.4	3.66	8.98	1779	65.4	65.2	2.79	9.45	2.05	22.2	21.8	142	243	26.9	116	10.5	4.71	2.59	150	78.7
5R	551.80	0.5–0.2	46.3	5.31	13.6	1141	84.7	85.4	4.00	13.0	2.64	28.7	30.9	168	109	20.4	131	6.91	5.87	3.14	80.3	52.3
9R	586.40	0.5–0.2	327	5.72	13.9	3348	140	129	8.56	28.0	6.54	61.0	35.1	178	59.3	17.1	135	16.4	6.77	6.88	121	58.5
10U	587.20	0.5–0.2	275	7.32	20.6	2729	205	170	14.2	33.6	11.3	79.7	38.8	177	123	27.2	150	13.6	11.6	6.11	114	71.2
10R	587.20	0.5–0.2	323	7.43	20.5	3097	227	196	9.24	28.3	5.77	63.4	42.8	194	54.4	19.6	153	15.2	11.4	6.94	119	53.4
10R-A	587.20	2–1	174	3.51	12.4	5819	94.9	79.9	15.8	33.6	23.1	58.5	21.0	186	188	36.2	160	25.9	5.53	5.91	391	95.2
10U-B	587.20	1–0.5	249	5.17	16.6	4930	145	121	15.8	38.1	16.8	73.0	29.9	198	166	36.8	161	23.3	8.60	6.76	279	94.9
10R-B	587.20	1–0.5	289	6.21	18.6	5610	164	134	17.1	39.8	19.9	73.9	30.7	195	168	37.4	172	23.7	8.64	6.84	282	94.8
10R-C	587.20	< 0.2	258	8.45	21.5	1692	230	179	13.1	31.1	11.5	63.2	38.1	146	223	17.9	122	8.08	11.3	5.01	56.2	46.6
3L	551.80	2–1	22.9	2.64	17.2	117	24.8	10.8	17.8	18.0	27.5	40.6	7.07	40.2	513	61.1	18.8	0.15	1.68	1.17	137	221
9L	586.40	0.5–0.2	59.5	3.82	20.0	115	51.7	26.0	31.2	26.3	31.8	45.0	7.10	28.2	349	46.7	23.7	0.09	1.06	0.74	32.4	114
10L	587.20	0.5–0.2	107	7.95	30.4	233	173	75.3	50.2	103	67.5	353	14.6	58.3	577	70.2	101	0.37	12.8	1.61	47.8	167
551WR[a]	551.80	Whole-rock	3.71	0.11	0.38	382	2.64	2.18	0.20	0.53	1.01	1.51	0.87	19.3	18.1	3.23	156	1.57	0.23	0.25	94.9	2.88
587WR	587.20	Whole-rock	13.7	0.60	3.00	3146	19.5	24.0	1.03	3.02	1.14	8.95	6.85	108	69.4	18.4	486	14.0	1.74	1.22	494	18.4
587WR-A[a]	587.20	Whole-rock	8.11	0.22	1.13	816	3.97	3.55	0.78	1.57	1.03	2.92	2.24	51.7	38.5	7.52	391	4.09	0.32	0.57	246	5.09
Woodleigh-1A (granitoid)																						
W1-WR	194.85	Whole-rock	81.1	1.17	35.2	14098	432	80.2	42.2	43.2	55.8	173	28.9	399	31.8	15.1	125	16.5	0.78	14.7	367	7.06
Yaringa-1 (sandstone)																						
Y1-1	355-K	< 2	58.0	10.3	17.1	4422	223	167	24.8	44.2	6.18	136	41.5	229	400	38.6	318	25.2	9.20	9.66	282	82.1
Y1-2	740-K	< 2	42.9	5.51	7.82	4057	176	1216	90.2	27.7	303	267	25.4	120	712	54.1	398	30.6	14.6	4.69	18567	164
Y1-3	2280-T	< 2	18.3	19.5	20.5	1086	74.0	108	14.7	22.8	5.28	82.8	39.2	147	1416	36.2	99.8	6.16	3.85	6.18	72.4	180
Y1-2WR	740	Whole-rock	3.17	0.20	0.75	246	5.48	22.1	2.03	1.29	7.15	6.34	1.54	18.5	50.9	5.59	50.4	1.62	1.52	0.39	1889	8.60
Y1-3WR	2280	Whole-rock	5.87	0.69	0.69	149	2.58	3.36	0.47	0.91	0.51	3.72	2.07	12.1	63.7	5.72	61.3	0.84	0.22	0.27	50.0	8.52
Yaringa East-1 (sandstone)																						
YE1-1	270.3-S	< 2	140	4.94	14.6	3692	141	110	19.5	54.1	24.6	76.7	28.8	168	88.7	31.6	166	18.4	5.34	7.53	125	65.8
YE1-2	273.6-S	< 2	219	5.99	18.4	4387	127	112	16.8	42.7	17.1	94.8	34.4	225	131	27.5	177	19.8	5.92	10.8	190	73.9
YE1-3	397.65-K	< 2	66.5	9.10	25.5	8951	238	117	19.3	48.2	102	143	46.0	191	1060	63.3	559	44.7	25.7	7.69	124	241
YE1-1WR	273.60	Whole-rock	63.9	1.78	8.72	2518	52.7	42.8	8.64	19.2	8.27	37.0	12.0	116	98.0	18.4	135	10.9	2.40	4.77	287	29.5
Coburn-1 (sandstone)																						
C1	401.8-K	< 2	16.6	3.23	7.10	1279	44.8	88.1	5.12	17.1	976	591	11.2	99.1	377	15.2	148	6.48	82.8	1.70	672	76.1
C2	1032.8-T	< 2	19.6	6.92	9.09	2455	120	164	9.38	32.6	4.41	267	34.6	224	285	21.7	100	12.7	11.54	10.8	176	33.9
Dirk Hartog-17B																						
DH	1487–1492-T	< 2	13.5	7.04	21.1	3066	314	586	3.53	24.1	40.4	39.0	42.7	124	479	19.9	547	20.2	32.9	3.73	89.5	66.6
Wandagee-1																						
WAN7	875–876	< 2	20.9	7.27	9.16	2115	125	160	9.58	34.0	6.39	273	36.3	231	260	20.4	96.2	10.9	12.0	11.3	165	28.3
WAN9	1010.70	< 2	9.48	6.67	19.2	2037	197	201	5.44	28.1	7.05	634	43.4	263	625	8.01	227	10.6	12.2	6.37	71.5	47.8
PAAS			75.0		16.0	1 wt. %	150	110	23.0	55.0	50.0	85.0	20.0	160	200	27.0	210	19.0	4.00	15.0	650	38.0

RSD relative standard deviation of AGV-1, *L* leachate, *U* untreated, *R* residue, *K* Kopke Sandstone, *T* Tumblagooda Sandstone, *S* Sweeney Mia Formation

[a] Clay content has been minimised by ultrasonic treatement

PAAS post-Archean average shales (Taylor and McLennan 1985)

Element correlations

Each element group mentioned above shows coherent behaviour, which is evident as significant positive correlations between individual element concentrations. The most strongly defined correlations are for samples from the diamictite, whereas the data from the sandstones are more scattered.

Some strong positive correlations among the transition metal group for the illites from the diamictite are: Cr–Sc ($R^2 = 0.92$), Cr–V ($R^2 = 0.98$) and Sc–V ($R^2 = 0.93$), and Co–Ni ($R^2 = 0.95$), Ni–Cu ($R^2 = 0.73$) and Co–Cu ($R^2 = 0.85$). The correlation between Cr and Ni is weaker ($R^2 = 0.54$).

Some strong correlations are also evident among the lithophile elements, for example Li–Cs ($R^2 = 0.92$), Rb–Cs ($R^2 = 0.80$), Li–Sn ($R^2 = 0.69$), Be–Sn ($R^2 = 0.77$), and Cs–W ($R^2 = 0.65$).

Remarkably, compatible ferromagnesian trace elements display significant positive correlations with some incompatible lithophile elements such as Cr–Be, Cr–Sn, Cr–Li, Ni–Cs, Ni–Rb, and Ni–W (Fig. 8).

Rare earth elements

In Fig. 9a, chondrite-normalised REE patterns of acid-leached residues and some leachates of the illites from the diamictite are presented. The REE patterns of the untreated illites from the diamictite and sandstones are shown in Fig. 9b, c. In addition, the REE pattern of PAAS is included in all REE diagrams. The REE pattern of the uplifted basement granitoid in the centre of the Woodleigh structure is also presented in Fig. 9b and that of the high-K basement granites from the Yilgarn Craton to the east of the study area is shown in Fig. 9c

Ce	Pr	Nd	Sm	Eu	Gd	Tb	Dy	Ho	Er	Tm	Gd	Tb	Dy	Ho	Er	Tm	Yb	Lu	Hf	Ta	W	Tl	Pb	Th	U
23.2	3.03	12.9	3.27	1.09	3.71	0.62	3.81	0.80	2.22	0.33	3.71	0.62	3.81	0.80	2.22	0.33	2.06	0.30	2.36	0.45	0.24	0.090	7.53	2.10	0.51
69.5	8.52	31.7	5.78	1.58	4.75	0.66	3.57	0.69	1.83	0.27	4.75	0.66	3.57	0.69	1.83	0.27	1.67	0.25	5.04	0.84	0.56		36.0	6.13	1.92
0.9	1.0	0.9	1.2	1.6	1.1	1.0	0.9	1.1	1.0	1.2	1.1	1.0	0.9	1.1	1.0	1.2	1.2	1.8	1.6	1.2	5.9		4.9	1.0	1.3
127	13.8	47.3	7.79	1.24	5.81	0.84	4.75	0.98	2.76	0.42	5.81	0.84	4.75	0.98	2.76	0.42	2.71	0.40	5.16	0.83	2.16	0.24	50.0	41.6	9.78
130	14.3	48.7	7.83	1.22	6.11	0.88	4.97	1.02	2.88	0.44	6.11	0.88	4.97	1.02	2.88	0.44	2.87	0.41	5.27	0.86	2.09	0.24	51.1	41.2	9.58
200	21.5	74.0	12.9	1.93	8.89	1.16	5.85	1.13	2.98	0.44	8.89	1.16	5.85	1.13	2.98	0.44	2.69	0.39	2.66	1.03	1.72	0.36	13.8	48.1	5.33
169	16.8	54.7	9.04	1.36	6.35	0.91	5.03	1.02	2.84	0.42	6.35	0.91	5.03	1.02	2.84	0.42	2.69	0.38	2.75	1.12	1.63	0.36	10.2	40.6	4.84
134	13.0	41.3	6.79	1.02	5.21	0.82	4.90	1.06	2.96	0.46	5.21	0.82	4.90	1.06	2.96	0.46	2.88	0.41	3.15	1.00	1.69	0.31	8.48	40.6	6.83
94.2	9.68	31.3	4.96	0.74	3.79	0.61	3.74	0.82	2.39	0.38	3.79	0.61	3.74	0.82	2.39	0.38	2.40	0.35	4.09	0.66	1.86	0.26	5.94	42.3	7.23
92.5	9.24	29.2	4.43	0.66	3.14	0.51	3.18	0.70	2.11	0.34	3.14	0.51	3.18	0.70	2.11	0.34	2.21	0.33	4.03	1.46	4.45	0.46	6.43	34.0	7.89
145	16.9	60.8	10.9	1.65	7.96	1.07	5.63	1.09	2.94	0.44	7.96	1.07	5.63	1.09	2.94	0.44	2.74	0.40	5.23	1.26	2.52	0.55	20.6	49.8	8.95
84.3	8.32	26.3	4.10	0.63	3.04	0.53	3.44	0.77	2.33	0.37	3.04	0.53	3.44	0.77	2.33	0.37	2.37	0.35	4.92	1.36	2.17	0.56	6.02	35.1	8.05
186	20.9	75.4	13.6	2.06	10.0	1.35	7.14	1.40	3.76	0.55	10.0	1.35	7.14	1.40	3.76	0.55	3.42	0.49	4.30	2.12	3.11	0.86	36.5	47.1	8.60
181	20.8	75.0	14.1	2.17	10.6	1.44	7.55	1.46	3.85	0.56	10.6	1.44	7.55	1.46	3.85	0.56	3.49	0.50	4.81	2.00	4.38	0.77	37.0	57.0	10.4
182	21.0	75.6	14.1	2.19	11.0	1.47	7.66	1.47	3.85	0.56	11.0	1.47	7.66	1.47	3.85	0.56	3.54	0.50	4.96	2.02	4.13	0.74	35.2	56.5	10.6
97.1	11.3	40.0	6.74	0.99	4.92	0.66	3.56	0.70	1.94	0.29	4.92	0.66	3.56	0.70	1.94	0.29	1.90	0.27	4.62	0.76	2.82	0.42	15.5	33.6	7.08
698	87.3	350	68.5	10.2	48.6	5.20	19.2	2.68	4.94	0.50	48.6	5.20	19.2	2.68	4.94	0.50	2.66	0.35	0.93	0.008	0.78	0.14	67.0	126	9.56
386	47.0	184	34.8	5.24	25.7	2.92	12.2	1.86	3.67	0.41	25.7	2.92	12.2	1.86	3.67	0.41	2.24	0.30	1.07	0.007	0.74	0.18	61.8	60.0	5.12
522	71.8	284	53.2	7.98	40.7	4.52	18.7	2.85	5.70	0.64	40.7	4.52	18.7	2.85	5.70	0.64	3.61	0.48	5.20	0.26	0.52	0.37	114.6	122	10.4
5.60	0.64	2.31	0.49	0.11	0.49	0.09	0.54	0.12	0.35	0.057	0.49	0.09	0.54	0.12	0.35	0.057	0.39	0.06	3.37	0.14	0.10	0.09	3.47	3.41	0.53
40.4	4.57	16.5	3.31	0.55	3.08	0.53	3.25	0.70	2.05	0.32	3.08	0.53	3.25	0.70	2.05	0.32	2.20	0.34	15.2	1.17	0.65	0.45	19.6	17.4	3.63
10.6	1.23	4.6	1.03	0.26	1.04	0.19	1.22	0.27	0.86	0.14	1.04	0.19	1.22	0.27	0.86	0.14	1.01	0.17	11.9	0.40	0.36	0.23	11.2	4.18	1.45
16.2	2.05	8.45	2.22	0.63	2.36	0.41	2.63	0.57	1.63	0.25	2.36	0.41	2.63	0.57	1.63	0.25	1.68	0.25	3.24	1.45	0.56	1.83	1.88	0.79	3.25
176	20.4	71.9	11.9	1.99	9.02	1.25	7.09	1.48	4.12	0.60	9.02	1.25	7.09	1.48	4.12	0.60	3.80	0.57	9.40	2.13	11.1	0.63	20.8	38.9	8.83
299	35.7	124	20.3	2.82	14.7	1.97	10.5	2.11	5.78	0.86	14.7	1.97	10.5	2.11	5.78	0.86	5.44	0.79	11.5	2.59	18.4	0.34	163	40.9	20.4
336	40.3	141	24.2	3.55	15.8	1.79	8.15	1.48	4.03	0.62	15.8	1.79	8.15	1.48	4.03	0.62	3.85	0.55	3.54	0.68	58.7	0.37	20.6	72.7	25.7
16.6	2.01	7.25	1.39	0.33	1.18	0.18	1.00	0.20	0.56	0.084	1.18	0.18	1.00	0.20	0.56	0.084	0.53	0.077	1.34	0.12	0.96	0.072	6.53	2.34	0.83
16.4	1.91	6.66	1.21	0.18	1.02	0.17	1.01	0.21	0.60	0.091	1.02	0.17	1.01	0.21	0.60	0.091	0.60	0.091	1.88	0.092	0.61	0.049	2.29	4.15	1.70
134	15.2	54.1	9.56	1.69	7.86	1.11	6.01	1.16	2.88	0.38	7.86	1.11	6.01	1.16	2.88	0.38	2.24	0.32	4.73	1.42	21.7	0.44	21.6	38.4	4.92
142	16.7	58.8	10.1	1.69	7.73	1.04	5.40	1.04	2.72	0.40	7.73	1.04	5.40	1.04	2.72	0.40	2.52	0.37	5.11	1.52	3.38	0.65	9.44	35.2	5.44
482	65.0	241	40.3	5.94	25.2	2.79	13.1	2.42	6.16	0.87	25.2	2.79	13.1	2.42	6.16	0.87	5.50	0.83	16.8	4.29	17.2	0.48	20.1	107	7.76
59.0	6.85	24.7	4.64	0.86	4.02	0.59	3.36	0.69	1.88	0.28	4.02	0.59	3.36	0.69	1.88	0.28	1.77	0.26	3.22	0.76	1.13	0.43	9.82	13.7	2.21
134	18.6	68.6	12.9	2.26	8.53	0.95	4.27	0.73	1.69	0.22	8.53	0.95	4.27	0.73	1.69	0.22	1.34	0.19	4.65	0.55	5.89	0.15	24.3	23.0	2.96
70.8	8.48	33.0	7.48	1.38	6.54	0.90	4.66	0.87	2.27	0.32	6.54	0.90	4.66	0.87	2.27	0.32	2.01	0.29	3.98	1.09	3.09	0.72	13.3	60.1	5.50
117	12.2	42.4	7.01	1.06	4.60	0.67	3.80	0.80	2.27	0.35	4.60	0.67	3.80	0.80	2.27	0.35	2.26	0.33	10.4	1.51	14.3	0.28	46.5	91.2	35.1
58.4	7.15	28.3	6.68	1.26	6.10	0.85	4.37	0.82	2.11	0.30	6.10	0.85	4.37	0.82	2.11	0.30	1.87	0.27	4.00	0.94	3.10	0.74	12.7	57.7	5.61
92.5	10.7	37.0	5.87	0.89	3.47	0.38	1.77	0.34	0.96	0.16	3.47	0.38	1.77	0.34	0.96	0.16	1.10	0.17	5.03	0.75	14.2	0.92	43.1	50.5	7.66
80.0	8.90	32.0	5.60	1.10	4.70	0.77	4.40	1.00	2.90	0.40	4.70	0.77	4.40	1.00	2.90	0.40	2.80	0.43	5.00	1.20	2.70		20.0	14.6	3.10

for comparison. The clays from this study are significantly enriched in light REE (LREE) relative to PAAS with La contents as high as 2.8×PAAS for the diamictite and 6.3×PAAS for the sandstones. The chondrite-normalised and averaged $(La/Lu)_c$ ratios of the illite residues (19.6) and the untreated illites (21.7) from the diamictite and the untreated illites from the sandstones (24) are higher than the $(La/Lu)_c$ ratio of PAAS (9.5). The untreated illites from the diamictite and sandstones have averaged $(La/Sm)_c$ ratios (4.9 and 4.4, respectively), which are similar to the $(La/Sm)_c$ ratio of PAAS (4.4), whereas the ratios for the illite residues from the diamictite are slightly higher (6.3). The opposite is the case for the $(Gd/Lu)_c$ ratios, where the averaged ratios of the illite residue from the diamictite (1.8) are close to the $(Gd/Lu)_c$ ratio of PAAS (1.4), whereas the averaged ratios of the untreated clays from the diamictite and sandstones are higher (2.4 and 2.9, respectively). Figure 9a clearly shows that the ratio of middle to heavy REE for the leachates are much higher than the ratio for the residues. Therefore the higher $(Gd/Lu)_c$ ratio for the untreated samples must be related to the contribution of the leachable phases. The significantly higher REE and Th contents of the leachates suggest that the leachable phases consist of mainly a phosphate-type acid-soluble mineral such as apatite or monazite: those samples (Y1-1, Y1-3, YE1-3 and DH) with highest concentration of P_2O_5 are most enriched in Th and REE (Tables 4 and 5).

Discussion

Petrography

Woodleigh is a proven impact structure (Mory et al. 2000; Reimold et al. 2003). Common PDFs in quartz, isotropization of quartz, and intensive fracturing of quartz clasts observed in the present study confirm the shocked metamorphism documented in earlier studies. The unsorted and chaotic structure of the diamictite indicates rapid deposition around the uplifted impact centre. However, it is not clear whether the diamictite is a primary crater-fill breccia or a secondary reworked gravity-flow deposit younger than the impact. Originally, parts of the diamictite may have been part of a polymict impact breccia with a clastic matrix containing shocked mineral and lithic clasts. Melt rocks are common in well preserved impact sites, and their remnants in the Woodleigh impact structure are represented by the rock fragments containing devitrified matrix (clays). Petrographic and SEM analyses show that illite is the main mineral component of the devitrified glassy fragments in the diamictite (Fig. 3c). Illite is also present in veins that clearly postdate the shock metamorphic textures as they cut across PDF-bearing quartz (Uysal et al. 2001b, 2002).

Geological significance of K–Ar and Rb–Sr data

The majority of illite fractions (except the <0.2 μm size fractions) from Ordovician and Devonian sandstones exhibit consistent K–Ar dates around ~400 Ma over a stratigraphic interval of about 2000 m. This indicates that illite crystallisation in the sandstones was a result of an episodic, short-lived thermal and fluid flow event, rather than one of progressive burial and that consequently the K–Ar dates are geologically meaningful. This thermal and fluid flow event predates maximum burial of the Southern Carnarvon Basin during the late Paleozoic and early Mesozoic (Ghori 1999). A regional tectonic event in the Late Silurian–Early Devonian, which could account for the illitization in the study area, is unknown in Western Australia to date. The Late Silurian–Early Devonian event reported elsewhere in Australia (e.g., Victoria in SE Australia) was related to the clockwise rotation of Gondwana and to the associated transcurrent movements as well as to the emplacement of mafic intrusions (Bierlein et al. 2001; Li and Powell 2001). However, the likelihood of similar events and the possible effects on thermal and fluid flow history in Western Australia need a further detailed examination through more regional geological and isotopic studies.

K–Ar ages around 360 Ma obtained for the coarser illite fractions from the diamictite agree with the Rb–Sr data. These results confirm illite K–Ar ages of ~360 Ma that were reported earlier and interpreted as reflecting the timing of impact-induced hydrothermal processes (Uysal et al. 2001b). The younger K–Ar values obtained mainly for the finer illite fractions from the sandstones and the diamictite indicate the effect of a Permian and Early Triassic thermal event, which is discussed in more detail in the following section.

Clay mineralogy and illite K–Ar ages: implications for the thermal history

Clay mineral authigenesis during sediment burial and hydrothermal events is broadly controlled by temperature (Srodon 1999). Here, illite and chlorite are the dominant clay mineral assemblages in the diamictite, together with a chlorite-rich mixed-layer; chlorite–smectite is also present in the diamictite. A temperature range of 170–250°C for the formation of these clays is estimated by analogy with other studies (Velde 1985; Pollastro 1993; Inoue 1995). Illite and chlorite also represent the main clay phases in the sandstones, but it has a lower IC indicating crystallisation at lower temperatures relative to illite in the diamictite (see below), as temperature is considered to be the main factor controlling IC in chemically homogenous environments (Kübler, 1964; Arkai 2002) and because the chemical compositions of illite from the diamictite and sandstone are close. The relationship between the IC values and K–Ar ages for the samples from the diamictite and sandstones might, therefore, provide valuable information on the thermal history of the Southern Carnarvon Basin and the Woodleigh impact structure. Better IC of illite in the diamictite suggests somewhat higher crystallisation temperatures at ~360 Ma relative to the illite of the sandstones reflecting lower temperature crystallisation at ~400 Ma. Previous studies have shown that the blocking temperature for clay-type minerals is close to their crystallisation temperature, which implies that any increase of the ambient temperature close to or beyond that of crystallisation would erase or, at least, affect the K–Ar systematics of previously formed illite (Clauer and Chaudhuri 1995). Therefore, the consistent set of most K–Ar dates of the illite from the sandstones indicates that these rocks have never experienced temperatures close to or above that reached during the ~400 Ma event, because their K–Ar systematics remained undisturbed. This relationship implies in turn that the thermal event with higher temperatures in the Late Devonian, recorded only in the illite from the diamictite, was a local process confined to the centre of the impact area. Several previous studies have documented impact-induced hydrothermal processes that were responsible for intensive alteration of target rocks and mineral authigenesis around the impact centre (e.g., Newsom 1980; Osinski et al. 2001; McCarville and Crossey 1994; Kirsimäe et al. 2002). The heat creating such hydrothermal systems is provided by shock-heated rocks including impact melt rocks and hot breccias. Indeed, the diamictite in the Woodleigh structure contains shocked rocks that may explain the temperature anomaly near the centre of the impact area.

Reconstruction of the regional thermal and burial history of the Carnarvon Basin indicate that the maximum burial was in the Late Permian–Early Triassic (Ghori 1999). Paleotemperatures of up to 130°C estimated for this event on the Gascoyne Platform obviously were too low to re-crystallise the coarser grained

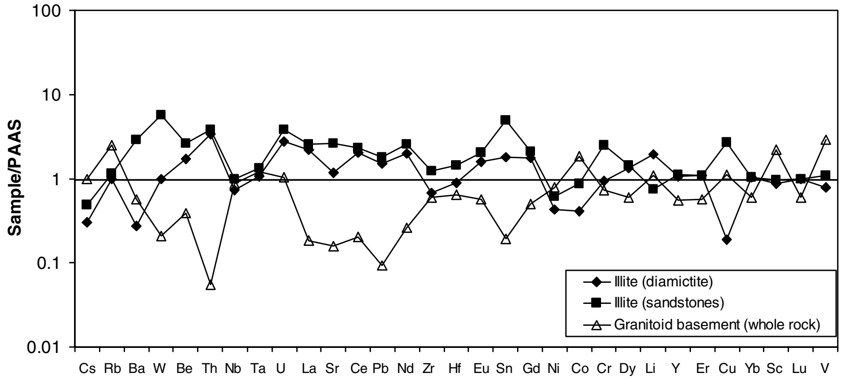

Fig. 7 PAAS-normalised trace element concentrations of averaged untreated clay fractions of different size fractions from the diamictite and sandstones compared with basement granitoid

Table 6 Avarage trace element ratios

	La/Th	La/Sc	Cr/Th	Co/Th	Th/Sc	Th/U
PAAS (1)	2.6	2.4	7.5	1.6	0.9	4.7
NASC (2)	2.5	2.1	10.1	2.1	0.8	4.6
Upper crust (3)	2.8	2.2	7.8	1.6	0.8	3.8
Phanerozoic greywackes (2)	2.9	1.3	6.7	1.7	0.5	5.0
Illites from Paris Basin (4)	3.5	2.5	23.9	1.5	0.7	5.0
High-K granites from Western Australia (5)	1.4	17.3	0.1		12.0	5.8
Woodleigh diamictite	1.0	6.1	1.0	0.1	6.2	4.7
Illites from Woodleigh diamictite	1.7	6.6	2.6	0.2	3.6	5.6
Carnarvon Basin sandstones	2.6	9.1	4.5	0.5	3.6	3.8
Illites from Carnarvon Basin sandstones	1.9	6.9	3.3	0.3	3.9	6.9
Woodleigh basement granitoid	8.9	0.2	101.0	53.1	0.02	0.2

(1) Taylor and McLennan (1985), (2) Gromet et al. (1984), (3) McLennan (2001), (4) Rousset and Clauer (2003), (5), Sheppard et al. (2003)

illite of the sandstones and diamictite, or to disturb their K–Ar systematics. However, the fine-grained illite from both the diamictite and the sandstone were affected by the Late Permian–Early Triassic thermal event, as it yields much younger K–Ar dates (Fig.4). Particularly, the less crystalline fine-grained illite from the sandstones was more susceptible to the younger thermal events than the better crystalline fine-grained illite from the diamictite (Fig.4), because the loss of radiogenic ^{40}Ar preferentially occurs in less-stable sheet silicates (Clauer and Chaudhuri 1999).

Significance of the trace element and REE results

Siderophile elements (e.g., Cr, Ni, Co) can be useful to verify the extraterrestrial contamination of clay-rich sediments related to meteoritic impacts (Koeberl 1998). Trace element concentrations, element ratios and the REE patterns of the illitic clays of different size fractions from the diamictite are very similar to those from the target sandstones. Specifically, the concentration of Cr, Ni and Co in the clays from the diamictite is similar to or even slightly less than the concentration from the sandstones. This suggests that the clays of the diamictite have inherited their elemental composition largely from the sandstones. Consequently, the trace element data provide no evidence of meteoritic contamination of the clays in the diamictite.

The trace element composition of authigenic clay minerals reflects the mineral/fluid partition coefficients for different elements, as well as the composition of fluids from which the clays precipitated. Trace element compositions and certain element ratios, therefore, can be useful as tracers of basinal and hydrothermal fluid chemistry. Some previous studies have used trace element and REE compositions of authigenic phyllosilicate minerals to characterise fluid compositions and monitor fluid flow events (e.g., Clauer et al. 1997; Zwingmann et al. 1999; Uysal et al. 2003; Heath and Campbell 2004). The most comprehensive trace element dataset for clays was previously reported for illite from the Paris Basin (Rousset and Clauer 2003), which is similar in its trace element concentrations and ratios to those of PAAS (Table 6). By contrast, the clays from the herein studied diamictite and sandstones are remarkably enriched in LREE and many other incompatible elements (Th, U, Li, Sn, Be, and W) relative to PAAS (Fig. 7). Furthermore, they show significantly high Th/Sc and La/Sc ratios and low La/Th and Cr/Th ratios compared to those of PAAS. Such geochemical characteristics indicate precipitation of the clays from fluids enriched in incompatible elements that are characteristic of continental crust rocks. At the same time, major element data show that most illites from this study are also somewhat enriched in compatible elements such as Fe and Mg (Fig. 6). Interestingly, the illitic clays show some unusual positive correlations between incompatible litho-

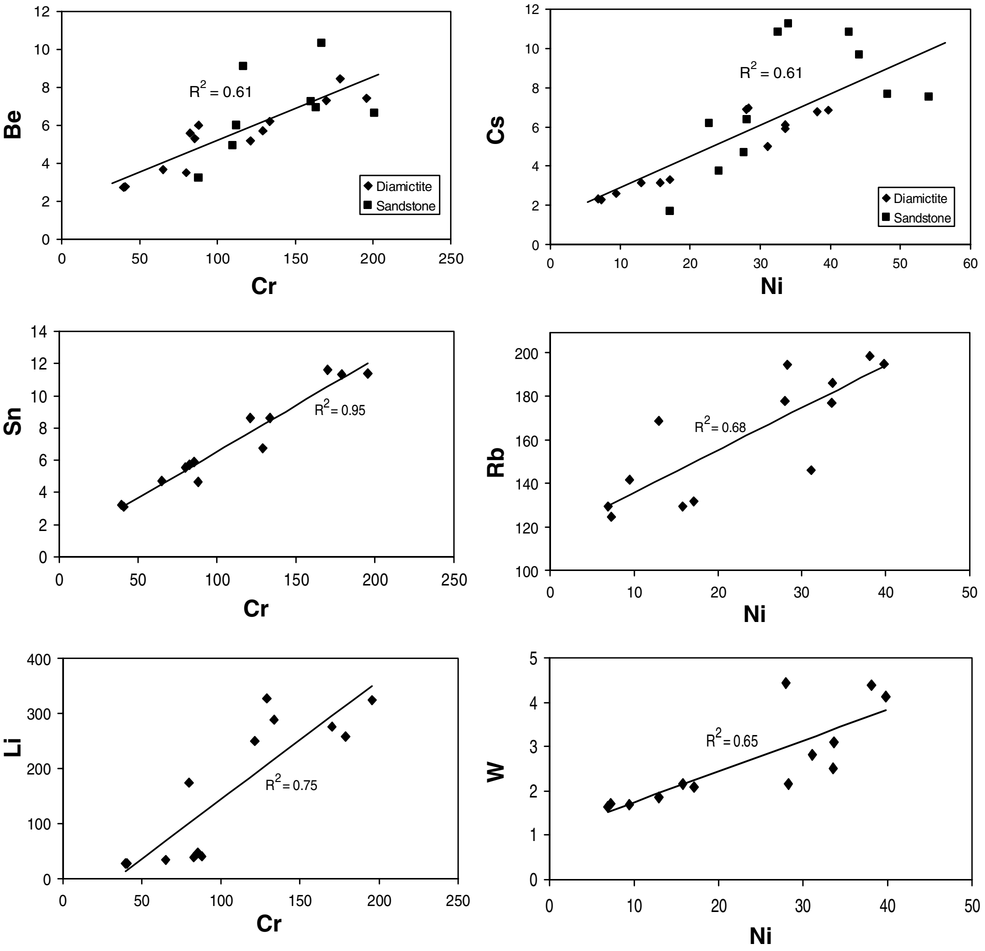

Fig. 8 Correlations between compatible ferromagnesian and incompatible lithophile elements. Correlations between Cr and Be (samples with anomalously high concentrations have been excluded) and Ni and Cs represent both the diamictite and the sandstones, whereas the rest of the correlations are only for the diamictite

phile elements and highly compatible ferro-magnesian trace elements (Fig. 8). These correlations suggest that higher incompatible element content accompanies a higher proportion of mafic input to the illite-forming fluids. Such remarkable trace element associations are unusual because of the different geochemical behaviour of compatible and incompatible elements during igneous rock forming processes.

The most likely scenarios for the source of the illite-forming fluids are summarised: the illite K–Ar ages of the coarse-grained illites from the sandstones indicate a thermal and fluid flow event during the Late Silurian–Early Devonian. Silurian–Devonian lamprophyres are widespread worldwide and an association of abundant mafic and felsic intrusions including lamprophyres of similar age have been reported in SE Australia (Rock et al. 1991; Vaughan 1996; Bierlein et al. 2001). Although not known in Western Australia to date, similar magmatic events and the presence of associated deep alkaline magmatic fluids may have affected the sedimentary basins in Western Australia. Alternatively, a more plausible explanation for the chemical composition of the illite forming fluids could be related to interactions of gravity-driven hot basinal fluids with alkaline mafic rocks from the elevated Archaean and Proterozoic Yilgarn Craton (Rock et al. 1991) to the east of the study area, or with such material transported and reworked in the studied sedimentary succession. Based on the paleocurrent data (Hocking 1991), the potential sources of the sandstones in the studied succession are the Palaeoproterozoic rocks that occur in the northwestern edge of the Yilgarn Craton, less than 100 km to the east of the study area. The paleocurrent data are consistent with the elevation of the Precambrian craton, which would control the gravity-driven fluid flow from the east towards the Carnarvon Basin.

Conclusions

Our petrographic, mineralogic, K–Ar and Rb–Sr isotopic and geochemical investigation of illitic clay minerals from clastic rocks in the Woodleigh impact structure and Carnarvon Basin provides important information about their evolution:

1. Diamictite near the centre of the Woodleigh impact structure contains shocked fragments and devitrified impact melt rocks derived largely from Ordovician–Devonian target sandstones. Illite is the main alteration mineral in the diamictite and the target sandstones.

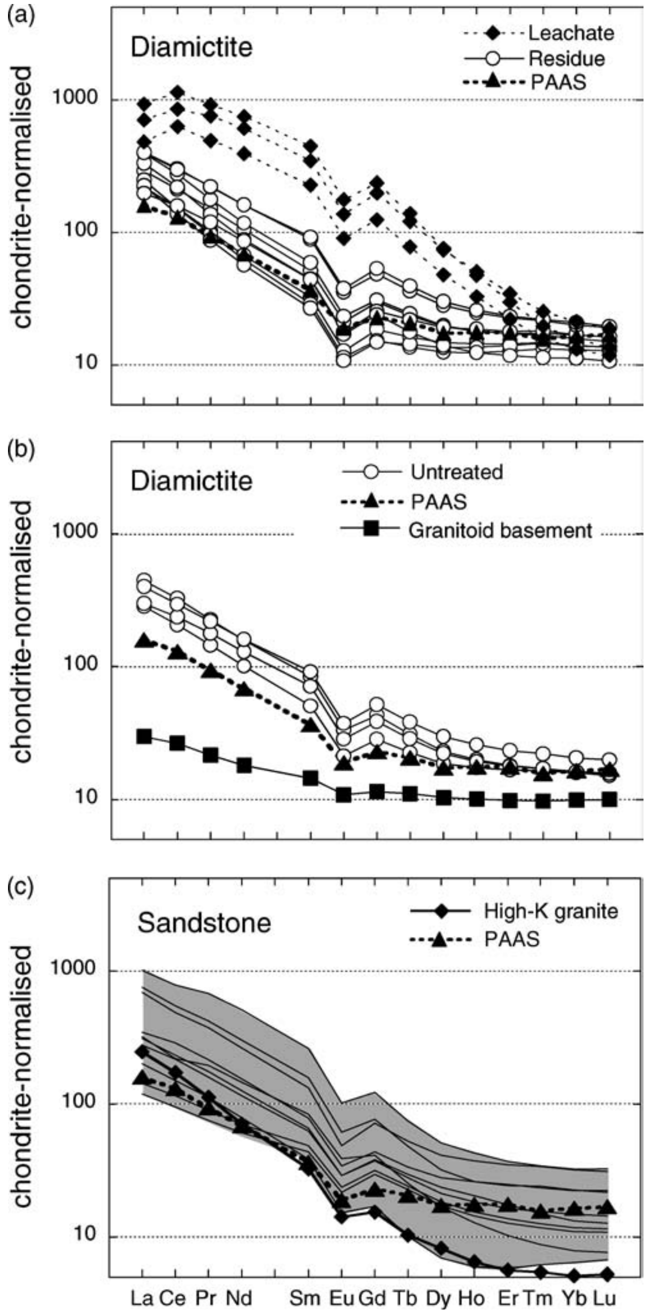

Fig. 9 REE patterns for the clay samples from the diamictite (**a** and **b**) and sandstones (**c** *shaded field*)

2. The illite precipitated initially in the sandstones may have formed in the Late Silurian–Early Devonian (K–Ar ages of ~400 Ma). Subsequent impact-induced hydrothermal processes in the Late Devonian (K–Ar and Rb–Sr ages of ~360 Ma) are considered to have caused recrystallisation of illite preserved in the diamictite and alteration of impact melt rocks at higher temperatures.
3. Illites from the diamictite and from the sandstones have very similar trace elemental compositions, suggesting that the clays in the former inherited their elemental composition largely from the latter.
4. Fluids from which the clays precipitated are compositionally enriched in incompatible lithophile elements and, to a lesser extent, in compatible ferromagnesian elements.
5. The source of chemical composition of the illite forming fluids is not well constrained. A possible and preferred explanation is the interaction of gravity-driven hot basinal fluids with Archaean and Proterozoic basement to the east of the study area, or with such material transported and reworked in the studied sedimentary succession.

Acknowledgements We thank Balz Kamber for the discussion and his assistance with the strontium isotope analyses. We acknowledge the technical assistance of Alan Greig for the REE analyses. We thank Irena Kinaev for technical assistance during the rubidium and strontium analyses. Analytical costs were covered by a UQ New Staff start-up and ARC research grants. Intellectual contribution of Andrew Glikson and and Tony Ewart and their critical comments on an earlier version of this paper are acknowledged. The paper was significantly improved by constructive and detailed reviews of Norbert Clauer, who is gratefully acknowledged. We are also deeply indebted to Alexander Deutsch for critical reviews from which the manuscript benefited. AJM publishes with the permission of the Director of the Geological Survey of Western Australia.

References

Allen CC, Gooding JL, Keil K (1982) Hydrothermally altered impact melt rock and breccia: contributions to the soil of Mars. J Geophys Res 87:10083–10101

Arkai P (2002) Phyllosilicates in very low-grade metamorphism: transformation to micas. Rev mineral geochem 46:463–478

Bierlein FP, Hughes M, Dunphy J, McKnight S, Reynolds P, Waldron H (2001) Tectonic and economic implications of trace element, ^{40}Ar/^{39}Ar and Sm–Nd data from mafic dykes associated with orogenic gold mineralisation in central Victoria, Australia. Lithos 58:1–31

Clauer N, Chaudhuri S (1995) Clays in crustal environments. Isotope dating and tracing. Springer Verlag, Heidelberg, Berlin, New York, p 359

Clauer N, Chaudhuri S (1999) Isotopic dating of very low-grade metasedimentary and metavolcanic rocks: techniques and methods. In: Frey M, Robinson D (eds) Low grade metamorphism. Blackwell Science, Cambridge, pp 202–226

Clauer N, Weber F, Gauthier-Lafaye F, Toulkeridis T, Sizun JP (1997) Mineralogical, geochemical (REE), and isotopic (K–Ar, Rb–Sr, δ^{18}O) evolution of the clay minerals from faulted, carbonate-rich, passive paleomargin of southeastern Massif central, France. J Sediment Res 67(5):923–934

Condie KC, Wronkiewicz DJ (1990) The Cr/Th ratio in Precambrian pelites from the Kaapvaal Craton as an index of craton evolution. Earth Planet Sci Lett 97(3–4):256–267

Deutsch A, Schärer U (1994) Dating terrestrial impact events. Meteoritics 29:301–322

Dypvik H, Ferrell RE, Sandbakken PT (2003) The clay mineralogy of sediments related to the marine Mjolnir impact crater. Meteorit Planet Sci 38(10):1437–1450

Eggins S, Woodhead JD, Kinsley, Mortimer G, Sylvester PJ, McCulloch MT, Hergt JM, Handler M (1997) A simple method for the simultaneous and precise analysis of 40 or more trace elements in geological samples by ICP-MS using enriched isotope internal standardization. Chem Geol 134:311–326

Faure G (1986) Principles of isotope geology, 2nd edn. Wiley, New York, p 589

Frey M (1987) Very low-grade metamorphism of clastic sedimentary rocks. In: Frey M (ed) Low temperature metamorphism. Blackie and Sons, Glasgow, pp 9–57

Ghori KAR (1999) Silurian–Devonian petroleum source-rock potential and thermal history, Carnarvon Basin, Western Australia. West Aust Geol Surv Rept 72, 88p

Heath CJ, Campbell IH (2004) A new geochemical technique for gold exploration: alkali element mobility associated with gold mineralization in the west Australian goldfields. Econ Geol 99(2):313–324

Hocking RM (1991) The Silurian tumblagooda sandstone, Western Australia. West Aus Geol Surv Rept 27, 124p

Iasky RP, Mory AJ, Blundell KA (2001) A geophysical interpretation of the Woodleigh impact structure, southern Carnarvon Basin, Western Australia. Geol Surv West Aust Rept 79, 41p

Inoue A (1995) Formation of clay minerals in hydrothermal environments. In: Velde B (ed) Origin and mineralogy of clays. Springer Verlag, Heidelberg, Berlin, New York, pp 268–321

Inoue A, Watanabe T, Kohyama N, Brusewitz AM (1990) Characterization of illitization of smectite in bentonite beds at Kinnekulle, Sweden. Clay Clay Miner 38:241–249

Kirsimäe K, Suuroja S, Kirs J, Karki A, Polikarpus M, Puura V, Suuroja K (2002) Hornblende alteration and fluid inclusions in Kardla impact crater, Estonia: evidence for impact-induced hydrothermal activity. Meteorit Planet Sci 37(3):449–457

Koeberl C (1998) Identification of meteoritic components in impactites. In: Grady MM, Hutchison R, McCall GJH, Rotherby DA (eds) Meteorites: flux with time and impact effects. Geol Soc London, Spec Publ 140:133–152

Kübler B (1964) Les argiles, indicateurs de metamorphisme. Rev Inst Fr Petrol 19:1093–1112

Lawrence SR, Cornford C (1995) Basin geofluids. Basin Res 7:1–7

Li ZX, Powell CM (2001) An outline of the palaeogeographic evolution of the Australasian region since the beginning of the Neoproterozoic. Earth Sci Rev 53(3–4):237–277

McCarville P, Crossey LJ (1994) Postimpact hydrothermal alteration of the Manson impact structure. Meteorit Planet Sci 29(4):499–500

Mory AJ, Iasky RP, Glikson AY, Pirajno F (2000) Woodleigh, Carnarvon Basin, Western Australia: a new 120-km diameter impact structure. Earth Planet Sci Lett 177:119–128

Mory AJ, Pirajno F, Glikson AY, Coker J (2001) GSWA Woodleigh 1, 2 and 2A, Woodleigh structure, Southern Carnarvon Basin. West Aust Geol Surv Rec 2001/6:147

Newsom HE (1980) Hydrothermal alteration of impact melt sheets with implications for Mars. Icarus 44:207–216

Odin GS, 35 collaborators (1982) Interlaboratory standards for dating purposes. In: Odin GS (ed) Numerical dating in stratigraphy. Wiley, New York, pp 123–149

Osinski GR, Spray JG, Lee P (2001) Impact-induced hydrothermal activity within the Haughton impact structure, arctic Canada: generation of a transient, warm, wet oasis. Meteorit Planet Sci 36:731–745

Pollastro RM (1993) Considerations and applications of the illite/smectite geothermometer in hydrocarbon-bearing rocks of Miocene to Mississippian age. Clay Clay Miner 41:119–133

Reimold WU, Koeberl C, Hough RM, McDonald I, Bevan A, Amare K, French BM (2003) Woodleigh impact structure, Australia: shock petrography and geochemical studies. Meteorit Planet Sci 38(7):1109–1130

Rock NMS, Bowes DR, Wright AE (1991) Lamprophyres. Blackie, Van Nostrand Reinhold, Glasgow, New York, p 285

Rousset D, Clauer N (2003) Discrete clay diagenesis in a very low-permeable sequence constrained by an isotopic (K–Ar and Rb–Sr) study. Contrib Miner Petrol 145(2):182–198

Sheppard S, Occhipinti SA, Tyler IM (2003) The relationship between tectonism and composition of granitoid magmas, Yarlarweelor Gneiss Comlex, Western Australia. Lithos 66:133–154

Srodon J (1999) Use of clay minerals in reconstructing geological processes: recent advances and some perspectives. Clay Miner 34:27–37

Srodon J, Eberl DD (1984) Illite. In: Bailey W (ed) Reviews in mineralogy, 13. Mineral Soc Am, 495–544

Steiger RH, Jäger E (1977) Subcommission on geochronology: convention on the use of decay constants in geochronology and cosmochronology. Earth Planet Sci Lett 36:359–362

Taylor SR, McLennan SM (1985) The continental crust: its composition and evolution. Blackwell, Oxford, p 312

Uysal IT, Golding SD (2003) Rare earth element fractionation in authigenic illite-smectite from Late Permian clastic rocks, Bowen Basin, Australia: implications for physico-chemical environments of fluids during illitization. Chem Geol 193:167–179

Uysal IT, Golding SD, Thiede DS (2001a) K–Ar and Rb–Sr dating of authigenic illite–smectite in Late Permian coal measures, Queensland, Australia: implication for thermal history. Chem Geol 171:195–211

Uysal IT, Golding SD, Glikson AY, Mory J, Glikson M (2001b) K–Ar evidence from illitic clays of a Late Devonian age for the 120 km-diameter Woodleigh impact structure, Southern Carnarvon Basin, Western Australia. Earth Planet Sci Lett 192:281–289

Uysal IT, Golding SD, Glikson AY, Mory AJ, Glikson M, Iasky RP, Pirajno F (2002) Reply to "Comment on: K–Ar evidence from illitic clays of a Late Devonian age for the 120-km diameter Woodleigh impact structure, Southern Carnarvon Basin, Western Australia". Earth Planet Sci Lett 201:253–260

Vaughan APM (1996) A tectonomagmatic model for the genesis and emplacement of Caledonian calc-alkaline lamprophyres. J Geol Soc 153:613–623

Velde B (1985) Clay minerals: a physico-chemical explanation of their occurrence. Elsevier, Amsterdam, p 427

Wise WS, Eugster HP (1964) Celadonite–synthesis, thermal stability, and occurrence. Am Miner 49:1031–1083

Yau YC, Peacor DR, Beane RE, Essene EJ, McDowell SD (1988) Microstructures, formation mechanisms, and depth-zoning of phyllosilicates in geothermally altered shales, Salton Sea, California. Clay Clay Miner 36:1–10

Zwingmann H, Clauer N, Gaupp R (1999) Structure-related geochemical (REE) and isotopic (K-Ar, Rb-Sr, $\delta^{18}O$) characteristics of clay minerals from Rotliegend sandstone reservoirs (Permian, northern Germany). Geochim Cosmochim Acta 63(18):2805–2823